Conformational Changes Occurring upon Reduction and NO Binding in Nitrite Reductase from *Pseudomonas aeruginosa*[†,‡]

Didier Nurizzo,[§] Francesca Cutruzzolà,[||] Marzia Arese,[||] Dominique Bourgeois,[⊥] Maurizio Brunori,[||] Christian Cambillau,[§] and Mariella Tegoni*[,§]

Architecture et Fonction des Macromolécules Biologiques, UPR 9039-CNRS, IBSM, 31 Ch. Joseph Aiguier, Marseille Cedex 20, France, Dipartimento di Scienze Biochimiche, Università di Roma "La Sapienza", P. le Aldo Moro 5, 00185 Roma, Italy, and ESRF, BP 220, 38043 Grenoble, France

Received June 8, 1998; Revised Manuscript Received July 27, 1998

ABSTRACT: Nitrite reductase (NiR) from *Pseudomonas aeruginosa* (EC 1.9.3.2) (NiR-Pa) is a soluble enzyme catalyzing the reduction of nitrite (NO_2^-) to nitric oxide (NO). The enzyme is a 120 kDa homodimer, in which each monomer carries one *c* and one d_1 heme. The oxidized and reduced forms of NiR from *Paracoccus denitrificans* GB17 (previously called *Thiosphaera pantotropha*) (NiR-Pd) have been described [Fülop, V., et al. (1995) *Cell 81*, 369−377; Williams, P. A., et al. (1997) *Nature 389*, 406−412], and we recently reported on the structure of oxidized NiR-Pa at 2.15 Å [Nurizzo, D., et al. (1997) *Structure 5*, 1157−1171]. Although the domains carrying the d_1 heme are almost identical in both NiR-Pa and NiR-Pd oxidized and reduced structures, the *c* heme domains show a different pattern of *c* heme coordination, depending on the species and the redox state. The sixth d_1 heme ligand in oxidized NiR-Pd was found to be Tyr25, whereas in NiR-Pa, the homologuous Tyr10 does not interact directly with Fe^{3+}, but via a hydroxide ion. Furthermore, upon reduction, the axial ligand of the *c* heme of NiR-Pd changes from His17 to Met108. Finally, in the oxidized NiR-Pa structure, the N-terminal stretch of residues (1−29) of one monomer interacts with the other monomer (domain swapping), which does not occur in NiR-Pd. Here the structure of reduced NiR-Pa is described both in the unbound form and with the physiological product, NO, bound at the d_1 heme active site. Although both structures are similar to that of reduced NiR-Pd, significant differences with respect to oxidized NiR-Pd were observed in two regions: (i) a loop in the *c* heme domain (residues 56−62) is shifted 6 Å away and (ii) the hydroxide ion, which is the sixth coordination ligand of the heme, is removed upon reduction and NO binding and the Tyr10 side chain rotates away from the position adopted in the oxidized form. The conformational changes observed in NiR-Pa as the result of reduction are less extensive than those occurring in NiR-Pd. Starting with oxidized structures that differ in many respects, the two enzymes converge, yielding reduced conformations which are very similar to each other, which indicates that the conformational changes involved in catalysis are considerably diverse.

Pseudomonas aeruginosa (*P. aeruginosa*) is a Gram-negative bacterium pathogenic to both animals and plants (*1*). It has been extensively studied and found to be resistant to most antibiotic families, due to the nonpermeability of its outer membrane to antibiotics and its ability to metabolize them. In anaerobiosis, *P. aeruginosa* can grow using nitrate (NO_3^-) as the final electron acceptor in the respiratory chain and thus participates in the biogeochemical nitrogen cycle (*2*). During the past few years, the nitrogen cycle (*3*) and especially the processes involved in denitrification have attracted some attention for three main reasons. First, gaseous derivatives of nitrate, such as NO and N_2O, participate in the destruction of the ozone layer. Second, denitrification is one of the fundamental problems to be solved in disposing of wastewater; nitrate and nitrite have to be removed before waste water can be released into the environment. Third, denitrification is responsible for the loss of nitrogen fertilizers from soils.

P. aeruginosa nitrite reductase (NiR-Pa) is a soluble protein located in the periplasmic space of the bacterium (*1*−*4*). In vitro, NiR-Pa catalyzes the four-electron reduction of oxygen, $O_2 + 4H^+ + 4e^- \rightarrow 2H_2O$ (*5*), and the monoelectronic reduction of nitrite, $NO_2^- + 2H^+ + e^- \rightarrow NO + H_2O$ (*6*). On the basis of biochemical and genetic data, it was concluded however that the reduction of nitrite is the physiologically significant process, its turnover number being much faster than that for O_2 reaction. Nevertheless, the four-electron reduction process has been studied as a model for terminal oxidases. To date, known nitrite reductases belong to three classes. (i) The class I reductases contain copper. (ii) The class II reductases carry two hemes, and NiR-Pa belongs to this class. (iii) The class III reductases carry six hemes. NiR-Pa is a homodimer with a molecular mass of 120 kDa, each monomer of which contains

[†] This work was supported by the CNRS-IMABIO program, by a EU BIOTECH Structural Biology project (BIO4 CT96-0281), by MURST of Italy (Programme Nazionale "Biologie Structurale" 1997), and by CNR ("Target Project on Biotechnology").

[‡] The coordinates have been deposited in the Brookhaven Protein Data Bank under access codes 1NNO and 1NRE.

* Corresponding author. E-mail: tegoni@afmb.cnrs-mrs.fr.

[§] UPR 9039-CNRS.

[||] Università di Roma "La Sapienza".

[⊥] ESRF.

S0006-2960(98)01348-8 CCC: $15.00
Published on Web 09/18/1998

one *c* heme and one d_1 heme (*7*, *8*), and where each cofactor is located in a distinct domain. The *c* heme is the electron-accepting pole and has been found in vitro to receive one electron from azurin or c_{551} with the same efficiency (*9*, *10*), although the c_{551} is the physiological donor (*11*). The d_1 heme is the site of reduction of oxygen (*12*, *13*) and nitrite (*8*, *14*).

The crystal structures of both oxidized and reduced NiR from *Paracoccus denitrificans* GB17 (previously called *Thiosphaera pantotropha*) (NiR-Pd) have been described (*15*−*17*), and the structure of oxidized NiR-Pa (NiR-ox) was solved in a previous study using molecular replacement with the coordinates of NiR-Pd as the starting model (*18*). The domains carrying the d_1 heme are almost identical in the oxidized NiR-Pa and NiR-Pd structures; the NiR-Pa *c* heme domain is similar to the classical class I cytochrome *c* fold, with His51 and Met88 as the axial ligands instead of the His17 and His69 present in NiR-Pd. In addition, the Met88-bearing loop in NiR-Pa, which was replaced by His17 in the NiR-Pd N-terminal segment, again showed a normal *c* type fold in our structure. Unexpectedly, in NiR-Pa the N-terminal of one monomer crosses the interface between the two monomers and is wrapped around the other monomer at the border of the two domains. This phenomenon is comparable to the "domain swapping" or "arm exchange" events previously observed in other systems (*19*, *20*) and may explain the cooperativity observed in NiR-Pa. The Tyr10 belonging to this N-terminal segment is hydrogen-bonded to a hydroxide ion, the sixth ligand of the d_1 heme iron, whereas Tyr25 (equivalent to Tyr10) is directly bound to the iron atom in the NiR-Pd structure. Important conformational changes were found to occur upon reduction and ligand binding in the NiR-Pd structure (*17*). In short, the *c* heme domain methionine-bearing loop returns to the normal class I cytochrome *c* fold, yielding the classical His/Met pattern of *c* heme coordination, and Tyr25 is expelled from its direct ligation partner, the iron atom of the d_1 heme. The results of the latter study showed that the enzyme reduction was under strong conformational control, and that there exist long-lived intermediates which were trapped by means of cryoquencing techniques.

In this study, we investigated the X-ray structure of the reduced NiR-Pa both unliganded and complexed with NO; these two enzyme forms were obtained by soaking the oxidized crystals in solutions containing ascorbate as an electron donor in the presence or not of the physiological substrate (NO_2^-). The redox state of the enzyme with and without NO (denoted NiR-NO and NiR-red, respectively) has been characterized microspectrophotometrically and correlated with the structural modifications observed. In the NiR-NO structure, the catalytic site of both monomers is occupied by NO. In both NiR-NO and NiR-red, the Tyr10 side chain, which interacted with the hydroxide ion (the axial ligand in the d_1 heme), is rotated around the Cβ−Cγ bond away from the active site. The hydroxide ion is replaced by the NO ligand in the NiR-NO structure, whereas the catalytic site is left empty in the NiR-red structure. The long loop between Lys56 and Pro62 is shifted toward the *c* heme and stabilized by two new hydrogen bonds. Although these conformational changes are significant, they are much less extensive than those observed in NiR-Pd. Along with the domain swapping mechanism, observed in NiR-Pa and not in NiR-Pd, these differences show how structurally homologous enzymes can exhibit considerable diversity in terms of conformational changes involved in their catalytic activity.

MATERIALS AND METHODS

Crystallization and Soaking Procedure. The protein used for the crystallization was purified using the method of Parr et al. (*21*). It had the suitable absorbance ratio in the oxidized state ($A_{640nm}/A_{520nm} = 1.0$, $A_{411nm}/A_{280nm} = 1.2$) and showed a single SDS−PAGE band. The crystallization conditions were the same as those described previously (*18*). Orthorhombic crystals ($P2_12_12$) were obtained in 2 M Na/K_2 phosphate and 50 mM Tris-HCl (pH 8.4) and had cell parameters of 163.2 Å × 90.4 Å × 112.0 Å. To prepare the reduced protein and the protein bound with NO, oxidized crystals were soaked for 10 min in reducing solutions containing 1 M sodium ascorbate or 100 mM ascorbate and 100 mM KNO_2 both in 2 M Na/K_2 phosphate and 50 mM Tris-HCl (pH 7.2). The crystals were then transferred for a few seconds to the cryocooling solution containing the previous mixtures in addition to 20% glycerol. All the solutions used for these experiments were previously saturated with Argon.

Microspectrophotometry. In the microspectrophotometric experiments, to measure the optical densities in the range of linearity (OD ≤ 2.5), the crystals that were used were thinner than those generally exposed to X-rays or the spectra were recorded in a range of wavelengths in which the extinction coefficients of the chromophores are low. The ORIEL microspectrophotometer, installed at ID09 ESRF beamline, consisted of a xenon lamp source and a CCD detector. The spectra were recorded with unpolarized light. Crystals were mounted on cryoloops on a goniometer head and maintained at 100 K by a cold stream of nitrogen gas (Oxford Cryosystems). The dark current corresponding to the electric noise was measured, and the baseline correction was performed with a buffer similar to that in which the crystals were soaked. Spectral processing (smoothing, displaying, and page setting) was performed with the IDL5.1 (Research System, Inc.) and Xmgr3.01 (ACE/gr Development Team) software. The crystal spectra of NiR-ox, NiR-NO, and NiR-red have been normalized at 529 nm, an isosbestic point in the oxidation−reduction transition.

Data Collection, Processing, and Structure Refinement. NiR-NO crystal X-ray diffraction data were collected at DESY (Hamburg, Germany) on the EMBL X11 beamline using a wavelength of 0.907 Å and a crystal−detector distance of 379.5 mm on a 30 cm Mar Research Imaging Plate (1° per image). NiR-red crystal X-ray diffraction data were collected at LURE (Orsay, France) on the W32 beamline with a Mar345 Mar Research Imaging Plate detector, using a wavelength of 1.105 Å and a crystal−detector distance of 340 mm (1.0° per image). Both data sets were processed with DENZO (*22*) and PrOW (*23*). They were merged with Scalepack (*22*) at a maximum resolution of 2.65 Å in the case of NiR-NO and with the CCP4 suite (Collaborative Computing Project 4, Daresbury Laboratory, U.K., 1979) at a maximum resolution of 2.70 Å in that of NiR-red.

The NiR-ox model at 2.15 Å resolution (*18*), without any ions or water molecules, was used as the starting model. After

Table 1: Data Processing and Model Refinement Statistics[a]

	NiR-NO	NiR-red
space group	$P2_12_12$	$P2_12_12$
resolution (Å^3)	15.0−2.65	12.0−2.90
no. of observations	361 716	401 690
no. of unique observations	44 018	36 815
R_{sym} (%) (overall/last shell)	11.0/56.9	9.4/42.0
$I/\sigma I$ (%) (overall/last shell)	10.3/2.1	5.2/1.8
completeness (%) (overall/last shell)	90.7/93.3	97.5/98.5
cell dimensions (Å)	166.1 × 88.1 × 114.0	166.6 × 89.0 × 112.9
V_m/solvent content (%)	3.47/64.6	3.49/64.7
no. of residues/solvent	1078/354	1074/78
R-free/*R*-factor (%)	24.4/20.1	23.4/21.1
residues in the most favored region of the Ramachandran plot (%)	83.4	83.6
rms on bonds (Å)	0.010	0.021
rms on angles (deg)	1.69	1.83
rms on dihedral angles (deg)	25.64	26.18
rms on improper angles (deg)	1.34	1.31
mean/rms on *B*-factors (Å^2)		
backbone	38.50/4.42	39.97/2.70
side chain	39.43/5.65	41.09/4.22
solvent	37.01/nd	33.98/nd

[a] The last shell resolutions were 2.71−2.65 and 2.98−2.90 Å for NiR-NO and NiR-red, respectively.

several cycles of the X-PLOR3.8.4.3 (*24*, *25*) rigid-body refinement procedure, each monomer domain was satisfactorily fitted. SigmaA-weighted maps ($2mF_o - DF_c$ and $mF_o - DF_c$) were calculated (*26*), with which the parts of the enzyme modified upon reduction and ligation were identified. Using the TURBO-FRODO graphics package (*27*) on a SGI workstation, the loop between residues 54 and 64 was reconstructed, the N terminus and Tyr10 were shifted, and the ligands were placed in patches of electron density which were visible at the d_1 heme catalytic site. The refinement, including some conjugate gradient and *B*-factor refinement cycles in X-PLOR3.8.4.3, was alternated with visual inspection and structural modifications on the screen. The final models of NiR-NO at 2.65 Å and NiR-red at 2.9 Å had *R*-free/*R*-factor ratios of 24.4%/20.1% and 23.4%/21.1%, respectively. The Ramachandran plot (*28*) indicated that more than 83% of the residues were in the most favored region and that none of them were in forbidden regions (Table 1). The refinement and stereochemical data are given in Table 1. The coordinates have been deposited with the Protein Data Bank with entry codes 1NNO and 1NNE for NiR-NO and NiR-red, respectively.

RESULTS AND DISCUSSION

Microspectrophotometric Characterization

To check whether any differences existed between the absorption spectra available in the literature (*8*) and those recorded on the microspectrophotometer described in Materials and Methods, a preliminary characterization of the enzyme in solution, in the oxidized and reduced states, was carried out in an X-ray capillary. Three main peaks were found in the spectrum of the oxidized enzyme (Figure 1, inset): the Soret band centered at 411 nm, the α-band of the *c* heme centered at 520 nm, and the broad α-band of the d_1 heme with a maximum at 640 nm. Upon reduction, the Soret band maximum shifted to 417 nm (not shown), with a shoulder at 460 nm, and the α- and *β*-bands of the *c* heme were resolved and centered at 523 and 552 nm, respectively. The maximum of the d_1 heme band shifted to 650 nm (Figure 1, inset). The ratio between the peaks was found to be consistent with that previously published in the case of the native enzyme (*8*). Prior to the collection of X-ray diffraction data, the redox and ligation states of NiR in the crystal were investigated by performing microspectrophotometric studies on cryocooled crystals. The absorption spectrum of an oxidized NiR crystal at 100 K (Figure 1, solid line) exhibited the same maxima as those obtained with the NiR-ox in solution. The spectra recorded at a cryotemperature between 500 and 700 nm showed bands that were resolved better than those observed at room temperature. It is worth mentioning that the similarity between the spectra obtained in solution and in the crystal suggests that the enzymes, especially the environment of the *c* and d_1 hemes, are likely to be comparable in the two physical states.

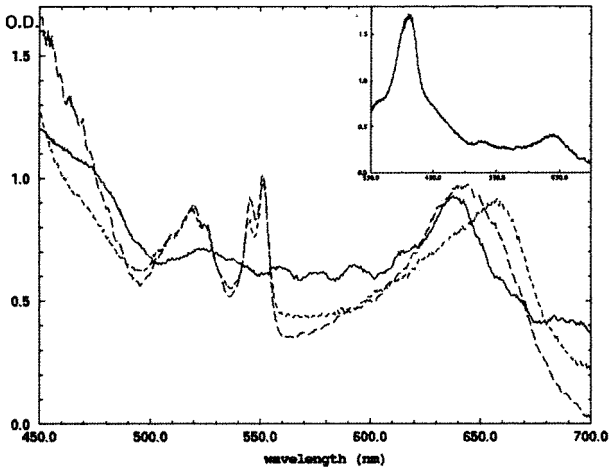

FIGURE 1: Optical microspectrophotometer spectra of NiR-ox (solid line), NiR-NO (dotted line), and NiR-red (dashed line) in the cryocooled crystals (100 K) between 450 and 700 nm. The spectra were recorded with unpolarized light. The crystal spectra of NiR-ox, NiR-NO, and NiR-red have been normalized at 529 nm, the isosbestic point in the oxidation−reduction transition. The inset shows the solution spectrum obtained with NiR-red.

Silvestrini and co-workers (*8*, *14*) have shown that NiR is able to reduce nitrite to NO in the presence of ascorbate. Indeed, the redox potential of ≈60 mV of ascorbate makes it a good electron donor for donation to the *c* heme, which has a redox potential of approximately 280 mV (*29*). The electron on the reduced *c* heme is then intramolecularly transferred to the d_1 heme, in a slow reaction. When nitrite is present at the d_1 heme site, its reduction is performed and NO is produced. At pH >6.2 and with ascorbate in excess, this reaction yields a "dead-end" species, in which the enzyme is completely reduced and NO is bound to the d_1 heme. At this pH, probably because of the deprotonated state of two histidines (327 and 369) at the active site, NO cannot be expelled (*8*).

To obtain crystals of NO-bound reduced NiR-Pa, we soaked the oxidized NiR-Pa crystals in a mother liquor

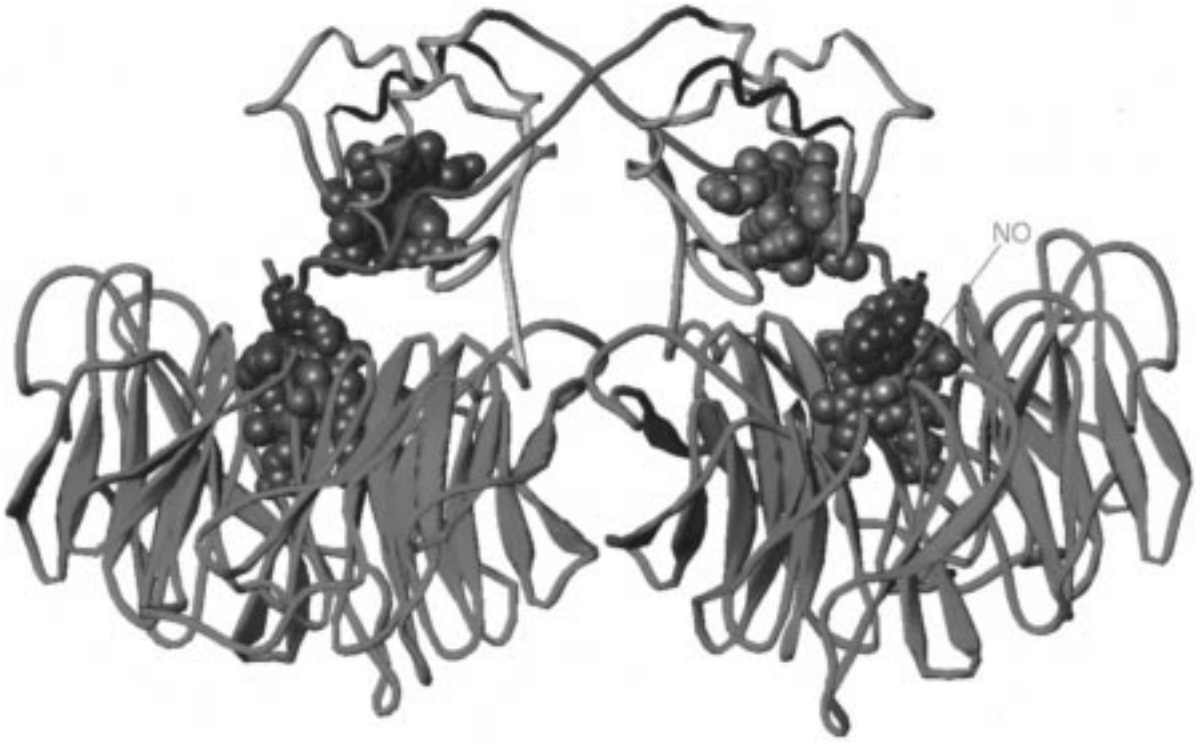

FIGURE 2: Ribbon picture of the of the Cα tracing of NiR-NO. The N terminus, the *c* heme domain, the linker, and the d_1 heme domains are blue, pink, yellow, and green, respectively. The atoms of the hemes and their ligands are shown in the form of CPK spheres.

containing 100 mM sodium ascorbate and 100 mM potassium nitrite, at pH 7.2, and recorded their spectrum with the microspectrophotometer (Figure 1, dotted line). As expected, the spectrum of NiR-NO was very different from that of the oxidized enzyme previously recorded; two peaks observed in the region between 500 and 600 nm were similar to the α- and β-bands of reduced cytochrome *c* (*30*) and the reduced NiR in solution (*8*). This close similarity demonstrates also that, at the experimental pH of 7.2, NO was not bound to the *c* heme of crystalline NiR-NO, since the maxima reported for this complex are at 534 and 568 nm (*8*). A third peak at 658 nm is different from the absorption maximum of the NO complex of the reduced d_1 heme at 648 nm (*8*). Nevertheless, the peak at 658 nm in the crystal was attributed to the α-band of the d_1 heme, since an experiment carried out with NiR in solution, under conditions as similar as possible to those used with the crystal (2 M phosphate), showed that the maximum in the d_1 heme peak shifted from 640 to 658 nm during the first few minutes after the addition of nitrite to the fully reduced enzyme; the shift was reversed after 30 min, and the maximum stabilized at 650 nm (F. Cutruzzolà and E. K. Wilson, personal communication). As previously noted with the other spectra in the crystal (Figure 1, solid line), the electronic transitions contributing to the α- and β-bands of the *c* heme in the spectrum of NiR-NO (Figure 1, dotted line) were better resolved than in solution; two shoulders were visible at 510 and 525 nm flanking the β-band maximum at 519 nm, and the α-band maximum was clearly split into two peaks at 545 and 551 nm.

To obtain reduced NiR crystals, a soaking procedure with 100 mM ascorbate but no nitrite was used. These crystals were characterized by a spectrum with two maxima in the 500−600 nm range corresponding to the reduced *c* heme peaks and the maximum of the d_1 heme peak centered at 642 nm, which was attributed to a partial reduction of the d_1 heme.

The ascorbate concentration was therefore increased up to 1.0 M. The α- and β-bands of the *c* heme were also found to be strictly superimposable on those of the crystals of NiR-NO (see above), while the d_1 heme α-band was somewhere between the maxima of the oxidized and reduced states in solution [640 and 650 nm (*31*)], which indicates that the level of reduction of the d_1 heme had increased but reduction was still incomplete (Figure 1, dashed line). In addition, the shoulder at 460 nm present in the reduced form in solution (*8*) and absent in the NO complex (*8*) was less defined in the spectrum of NiR-red in the crystal; whether this shoulder was completely hidden by the high absorption of the Soret band, or shifted at the cryocooling temperature that was used, cannot be determined.

NiR-Pd crystals have also been characterized by time-resolved microspectrophotometry following the reduction by dithionite and reoxidation by nitrite (*17*). The absorption maxima for the completely oxidized NiR-Pd (*17*) were reported to be identical to those observed for NiR-Pa, contrary to what might be expected to occur with enzymes having different heme axial ligands. However, a closer inspection of the 600−700 nm region in the published microspectrophotometric spectra clearly shows features different from those of NiR-Pa: in particular, a split α-band absorption for the oxidized d_1 heme, which is in accord with the solution spectra published by the same authors (*32*), and a blue shift of the same α-band absorption upon reduction.

X-ray Structure of the Reduced Form Bound to NO

Overall Structure. On the basis of the microspectrometric study, the crystals containing the reduced species bound to

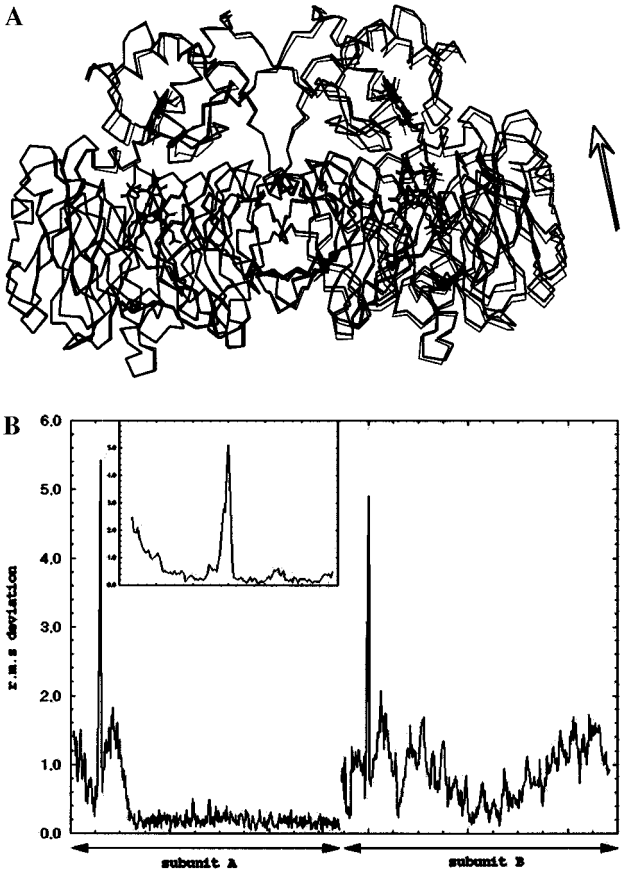

FIGURE 3: Overall movements of NiR-Pa upon reduction. (A) Cα trace of the NiR dimers with NiR-NO in thick lines and NiR-ox in thin lines, showing the rotation of the second monomer with respect to the first one. (B) rms deviation plots (in angstroms) of the Cα atoms of NiR-NO vs those of NiR-ox resulting from superimposition of only the d_1 domains of monomers A. The inset shows the superimposition of the N-terminal and *c* heme domains showing the drift of the N terminus and the movement of the 56−62 loop resulting from reduction.

NO were subjected to X-ray diffraction. The cryocooled NiR-NO crystal did not diffract at a resolution >2.65 Å, which is significantly lower than that at which the oxidized enzyme diffracted (2.15 Å). Generally, the structure of NiR-NO (Figure 2) is similar to that obtained with the oxidized form (*18*).

The structure of NiR-NO was superimposed on that of the A monomer of the oxidized NiR-Pa, including in the calculation the Cα atoms of the d_1 heme domains (Figure 3A). On the basis of this superimposition, the rms deviations calculated between all the Cα atoms of NiR-ox and NiR-NO indicate that significant deviations of the domains not used in the superimposition had taken place (Table 2 and Figure 3B). One complete monomer was found to have rotated 1−2° anticlockwise relative to the other, yielding a maximum shift of approximately 2 Å (Figure 3A). Within each monomer, the *c* heme domain was found to have rotated clockwise around the $c-d_1$ hinge, leading to shifts as large as 2 Å. An excellent superimposition was observed between the reduced and oxidized *c* heme domains taken alone, with the exception of the N terminus (residues 6−21) and a loop (residues 56−62) (Figure 3B and further in the text). The relative position of the hemes in a monomer is not changed in NiR-NO in comparison with the structure of NiR-ox, whereas the Fe−Fe or edge−edge distance varies by 0.1−0.5 Å, depending on whether two hemes of the same monomer or different monomers are taken into consideration.

Table 2: rmsd Calculated (A) between NiR-NO and NiR-ox, and NiR-NO and NiR-red, after Superimposition of the Cα Atoms of Only the d_1 Heme Domain of Monomer A and (B) between Superimposed Isolated Domains

		NiR-NO and NiR-ox	NiR-NO and NiR-red	NiR-Pa and NiR-Pd
		A		
c heme domain	monomer A	1.48	0.46	
	monomer B	1.54	0.88	
d_1 heme domain	monomer A	0.19	0.17	
	monomer B	1.05	0.88	
dimer		0.93	0.64	
reduced/reduced	*c* heme domain			sub A 5.90 sub B 2.28
	d_1 heme domain			sub A 0.62 sub B 2.66
		B		
c heme domain	monomer A	1.01	0.23	
	monomer B	0.96	0.27	
d_1 heme domain	monomer A	0.19	0.17	
	monomer B	0.18	0.16	
reduced/reduced	*c* heme domain			sub A 0.59 sub B 0.60
	d_1 heme domain			sub A 0.62 sub B 0.68

d_1 Heme Domain. The d_1 heme domain (from Gln149 to Tyr536) has an eight-blade β-propeller fold (Figure 2). Each blade is formed by a β-sheet composed of four antiparallel β-strands. The d_1 heme is located in the cavity at the center of the propeller, in front of the *c* heme. The proximal ligand is His182 on the side of the heme opposite from the catalytic site.

The presence of a molecule of NO at the catalytic site of both monomers could be unambiguously interpreted in the electron density maps (Figure 4A). The N atom of the NO molecule is directly linked to the iron atom of the d_1 heme (1.8 Å), and has replaced the hydroxide ion found in the NiR-ox structure. The N−O distance has been fixed at 1.15 Å, as found in the Cambridge Data Bank. The angle formed by Fe−N−O was found to be 135°, which is lower than the expected 180°, but somewhat closer to it than the value found in sperm whale myoglobin [112° (*33*)]. In the case of CO binding to hemoglobin or myoglobin, the deviation from the expected value of 180° has been proposed to result from the interaction of the apoprotein with the ligand, as a means of modulating the affinity for the poisonous product (*33*, *34*). A bent conformation is also found in d_1 heme models complexed to NO (*35*). The oxygen of NO interacts in the distal pocket of NiR-NO with two histidines, His327 and His369 (at a distance of 3.4 and 2.6 Å, respectively; Figure 4B), which were proposed to be involved in the dehydration of the substrate at the catalytic center (*15*, *18*).

A rotation of the Tyr10 side chain is also observed, resulting in a 4.2 Å shift of the tyrosine OH group (Figure 4B). The environment of the d_1 heme in its cavity was not affected by the reduction, however, and in particular the residues of the apoprotein interacting with the metal and the porphyrin are the same in NiR-NO as those involved in NiR-ox (*18*). The planarity and the orientation of the d_1 heme were not affected, contrary to what has been found to occur in NiR-Pd (*15*−*17*). The structure of reduced NiR-Pd resulting from the reaction with the substrate, NO_2^-, has been

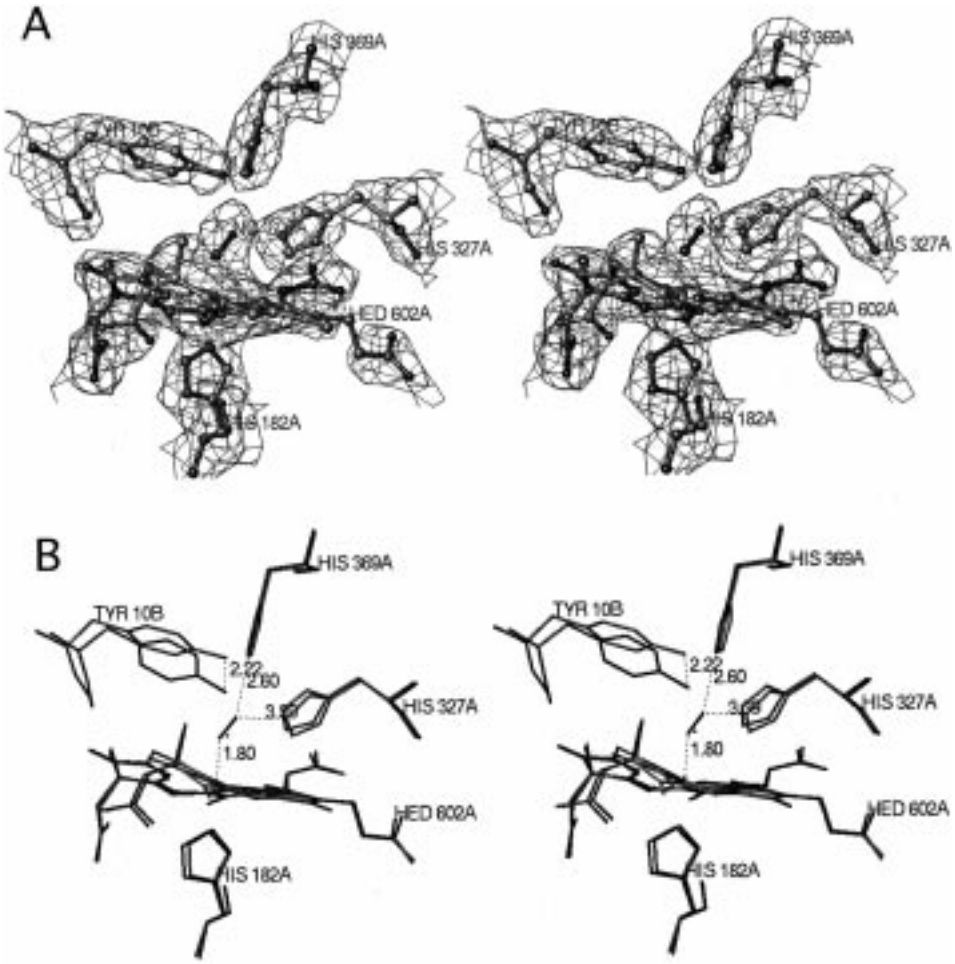

FIGURE 4: d_1 heme catalytic site with NO bound. (A) Electron density map of the catalytic crevice, comprising the d_1 heme, the NO bound to the d_1 iron atom, and the neighboring residues. (B) Stereoview of the superimposed d_1 heme catalytic sites of NiR-ox (red) and its bound OH^- (black circle) and NiR-NO (atom type colors) with NO bound and the stabilizing residues. Tyr10 and OH^- shifted upon reduction.

solved, and NO and NO_2^- were visible at the active d_1 site of monomers B and A, respectively (*17*). The position of the product, NO, is only slightly different from that found in NiR-Pa. The distance between Fe and N was larger in the former, 2.02 Å; the angle formed by Fe−N−O was found to be 131°, and the N−O binding distance was fixed at 1.37 Å. The values mentioned for NiR-Pd are in line with those previously found in *Lupinus luteus* leghemoglobin in the presence of NO [Fe−N distance of 1.97 Å and N−O distance of 1.35 Å as directly measured with the coordinates (PDB entry 1GDL)], whereas the values that we have mentioned above in the case of NiR-Pa are very close to those published for sperm whale myoglobin whose structure with bound NO was solved [Fe−N distance of 1.89 Å and N−O distance of 1.15 Å (*34*)].

c Heme Domain. The fold of the *c* heme domain (from Asp30 to Gln115) contains four α-helices with an arrangement similar to that observed in the classical type I cytochrome *c* (*36*). This domain is the physiological electron acceptor pole, which receives electrons donated by cytochrome c_{551} (*11*). The *c* heme is maintained in the heme crevice by covalent bonds at Cys47 and Cys50. The axial ligands are those usually found in cytochrome *c*, His51 and Met88, and they remain unchanged upon reduction, contrary to what was found to occur in NiR-Pd (*17*). As expected on the basis of the optical spectrum, no patches of electron density that can be attributed to the presence of NO in the nearby environment of the *c* heme were observed, confirming that NO binding to the *c* heme does not occur at this pH value.

After superimposition with NiR-ox, a significant deviation was observed in the loop between residues Lys56 and Pro62, which is displaced 6 Å (Figures 5 and 6A). This loop is close to the *c* heme and the consensus sequence for the *c* heme's linker segment, Cys47-(Ala-Gly)-Cys50-His51. In the oxidized form, the 56−62 loop performs a large turn (Figure 5), which is constrained by a hydrogen bond between the backbone atoms of Arg55 and Leu63. In NiR-NO, this turn is tighter and shorter due to a new hydrogen bond established between the CO group of Gly60 and the NH group of Ala58. A topology which does not commonly occur in turns is observed, since the NH of the first residue (Gly60) interacted with the CO of residue $i - 2$ (Ala58). Other hydrogen bonds were established between the CO of Lys61 and the Nδ of His51 and between the Lys61 side chain and a propionate group of the *c* heme. In the whole rearrangement, the OH group of the Thr59 side chain moved 4.65 Å and established a new hydrogen bond with Gln11 of the swapped N-terminal segment of the other monomer. A second significant deviation was detected at the N terminus; in fact, when this segment is included in the superimposition of the *c* heme domains, a deviation is observed, with an increasing rms value, working backward to the N terminus (Figure 3B, inset). This may have been due to the relative

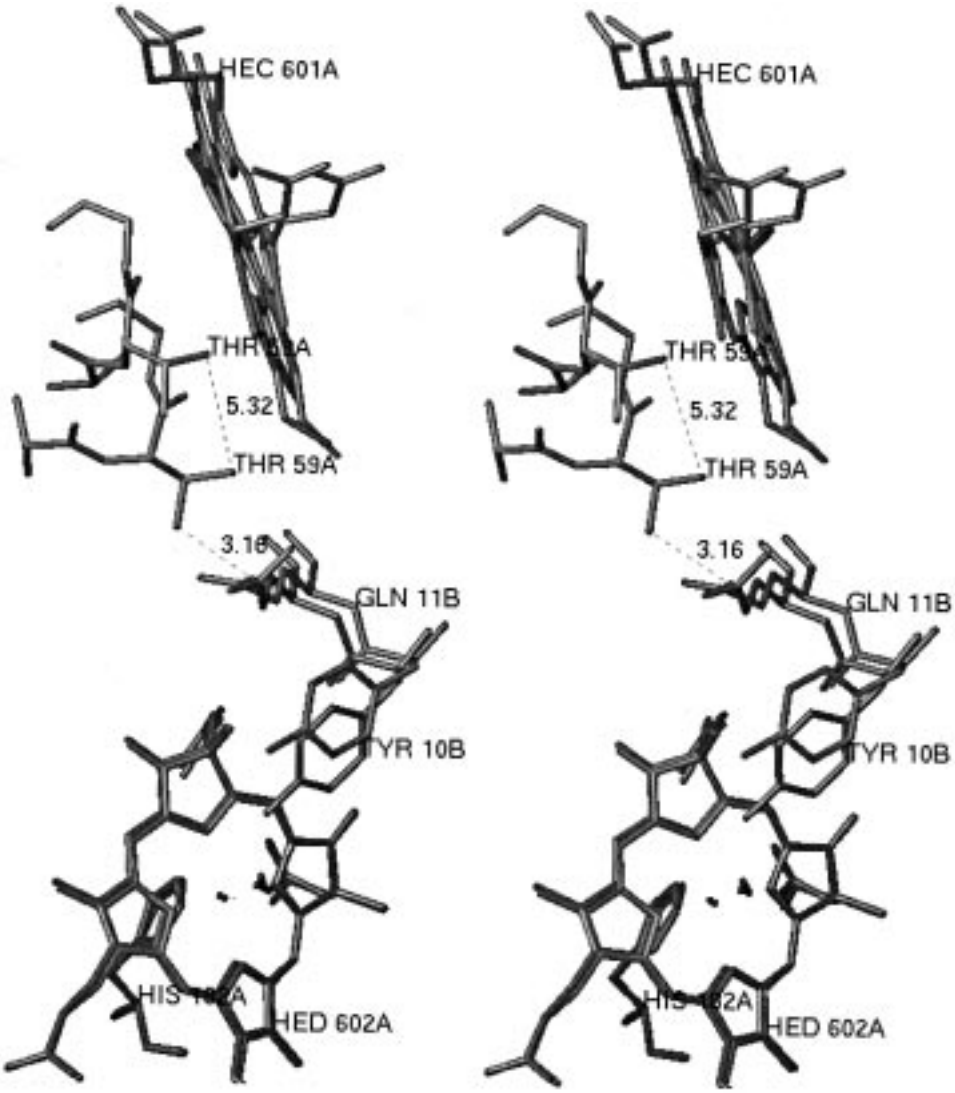

FIGURE 5: Stereoview of the conformational change in the 56A−62A loop upon reduction. NiR-ox is red and NiR-NO green. The two hemes are displayed as well as the hydrogen bond between Thr59A and Gln11B and the rotation of Tyr10B.

movement of the *c* heme and d_1 heme domains, which in turn may have resulted from the new hydrogen bonds from Thr59A to Gln11B and from Thr59B to Gln11A, and therefore from the movement of the loop described above.

Unbound Reduced Form

The reduced crystals of NiR-Pa in the absence of ligand diffracted only to a resolution of 2.9 Å. The overall structure of NiR-red could be superimposed on that of NiR-NO with a rms deviation of 0.17 Å, taking one of the d_1 heme domains into account in the calculation (Table 2). As in the case of NiR-NO, the relative orientation of the hemes did not change and their distance varied by no more than 0.1−0.4 Å. The absorption spectra of NiR-red in the crystal showed that in the dimer, both *c* hemes were reduced. The position of the d_1 heme band maximum between 640 and 650 nm (corresponding to the fully oxidized and the fully reduced d_1 heme, respectively) indicates that in the crystal these prosthetic groups are not fully reduced, however. In the X-ray structure, monomer A upon reduction has undergone structural modifications strictly identical to those described above in NiR-NO. The 56A−62A loop is in the "reduced" conformation, and Thr59A establishes a hydrogen bond with Gln11B. The Tyr10B side chain rotates, leaving the catalytic site open for the binding of a ligand. No patches of electron density were observed near the Fe of the d_1 heme, which indicates that no hydroxide ions were bound to it any longer. The movement of the 56B−62B loop, which has formed the new hydrogen bond with Gln11A, is also observed in monomer B, as well as the rotation of the side chain of Tyr10A at the catalytic site. However, a Fourier difference peak was observed near the Fe atom of the d_1 heme in monomer B, with a shape quite comparable to that identified as a hydroxide in the NiR-ox structure calculated at the same resolution. The latter structural feature suggests that the d_1 hemes in monomers B might be only partially reduced, if at all, in the crystal lattice. The putative oxidized state of the second d_1 heme might originate from the fact that (i) it has not been reduced or (ii) it has been reduced and then immediately reoxidized by traces of oxygen. The existence of a positive cooperativity between the two d_1 hemes, reported by Blatt et al. (*31*), and the fact that a completely reduced NiR-NO structure was obtained, might support the second hypothesis. The oxidized state of monomer B might be due to the reoxidation of the d_1 Fe in the presence of traces of oxygen, a reaction that does not take place when

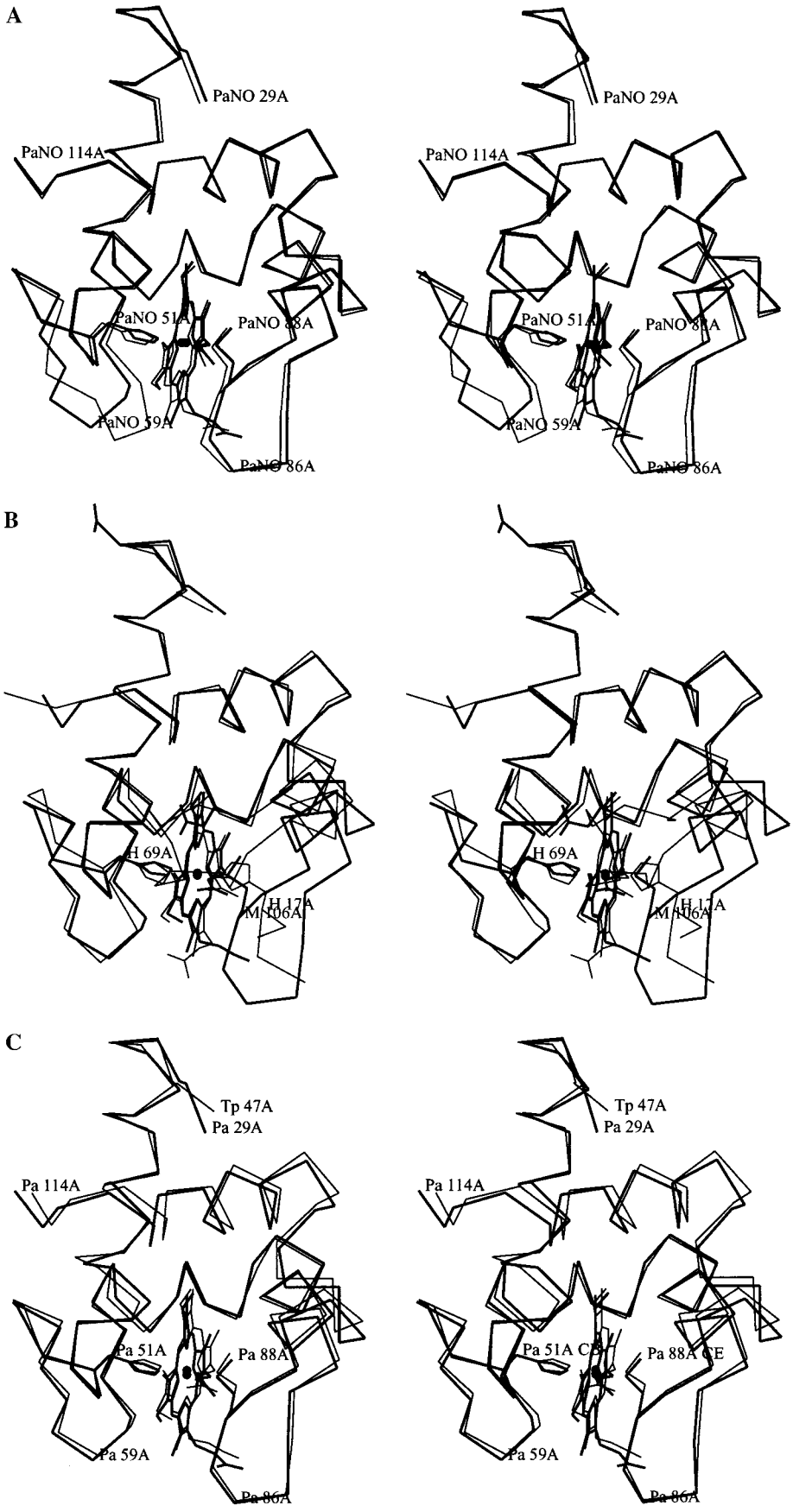

FIGURE 6: Stereoviews of comparisons between *c* heme domains after superimposition (the scales and orientations are kept): (A) NiR-NO (thick line) compared to NiR-ox (thin line), (B) NiR-Pd-red (thick line) compared to NiR-Pd-ox (thin line), and (C) NiR-Pa-NO (thick line) compared to NiR-Pd-red (thin line, Tp).

NO is bound and blocks the d_1 heme in its reduced form. Whatever the processes involved, the structures obtained by X-ray crystallography always give an average picture of all the molecules in the crystal; the fact that one monomer can be identified as being different from the other, as compared to an average situation observed between monomers A and B, is quite puzzling. The only possible explanation here might involve crystal packing considerations, taking into account the effects of not only simple steric hindrance but also stereoelectronic influence.

Comparison with the cd_1 NiR from P. denitrificans GB17

The only other cd_1 NiR structure described to date is that of *P. denitrificans* GB17. As expected from sequence comparisons, most of the structural differences between NiR-Pd and NiR-Pa have been detected in the *c* heme domain and in the N-terminal segment (*18*). In the oxidized state, the NiR-Pd *c* heme is axially coordinated by His17 and His69, while the canonical axial ligands for *c* heme cytochromes are Met and His, as was found to be the case in NiR-Pa (Figure 6B,C). The N-terminal arm is interchanged between monomers A and B in Nir-Pa, while it stays on the same monomer and wraps around the *c* heme domains in NiR-Pd. These differences in the N-terminal arm conformations enable the Tyr25 and Tyr10 side chains to become the axial ligand of the d_1 hemes of NiR-Pd and NiR-Pa (via a hydroxide ion), respectively.

Kinetic structural studies on NiR-Pd have been published in which the reaction pathway of the reduction of nitrite to nitric oxide has been described (*17*). The eight-blade β-propeller fold characterizing the d_1 heme domain seems to be conserved among all cd_1 NiRs belonging to class II (*17*). No significant shift of the backbone was observed in the d_1 domains of NiR from Pd or Pa upon reduction. Furthermore, their reduced d_1 domains were found to be very similar, with a rms deviation of only 0.62 Å among the 408 residues (Table 2).

The structural changes in the NiR-Pd *c* heme domain occurring upon reduction were extremely conspicuous in comparison with those observed in the d_1 domain and the *c* domain of NiR-Pa upon reduction: the His17−His69 *c* heme coordination became a Met106−His69 coordination, because the N-terminal arm had moved out of the *c* heme neighborhood, and because of the shift of the loop (residues 99−116) bearing Met106 toward the *c* heme (Figure 6B). In the reduced NiR-Pd, the N-terminal tail, before Gln26 had moved, was flexible and was not visible in the electron density map; due to this shift, Tyr25 did not coordinate the d_1 heme any longer, but was replaced by ligands such as NO_2^-, NO, and SO_2^- (in the presence of dithionite). It is important to underline that, despite the fact that the changes observed in NiR-Pd were tremendous in comparison with those which occurred in NiR-Pa, the resulting reduced enzymes are very similar at the level of the *c* heme. The structures of the *c* heme domains of the two enzymes superimpose perfectly, including the 55−60 loop, which had shifted from oxidized to reduced in NiR-Pa; the resulting rmsd between the two structures on the 86 Cα atoms of the *c* domains was only 0.6 Å (Figure 6C and Table 2).

Concluding Remarks

By contrast with the extreme diversity observed between the oxidized forms, the reduced forms of NiR-Pa and NiR-Pd are very similar, apart from their N-terminal tails. In both cases, the large (NiR-Pd) or small (NiR-Pa) movement of the N-terminal arm seems crucial for making the Fe of the d_1 heme accessible to the substrate or to a ligand. In NiR-Pa, where the reduced form is more clearly defined at the N terminus, a cascade of events might explain how the observed shifts correlate with catalysis. The reduction of the *c* heme seems to induce the 55−60 loop movement, which may help Tyr10 to move away from the hydroxide bound to the d_1 Fe(III) and allow formation of a hydrogen bond between Thr59 and Gln11 (of the other monomer); this appears to be a crucial event in the opening of the d_1 heme distal pocket. Our comparison between NiR-red and NiR-NO led to the conclusion that Tyr10 shifts prior to the reduction of the d_1 Fe(III) to Fe(II) since it is displaced in the X-ray structure from crystals which are not fully reduced. The last step may therefore be the electron transfer from the *c* heme Fe(II) to the d_1 heme Fe(III), followed by the expulsion of OH^- and the binding of NO_2^-. The initial kick of the 56−62 loop is difficult to explain; however, the stabilization of the 56−62 loop by Gln11 may explain why two different conformations were observed in the oxidized and reduced forms. No conformational switch of this kind has ever been observed to date in bacterial cytochromes *c* of class I upon reduction. Moreover, the stabilization mentioned above and involving residue 11 cannot take place in the cytochromes of class I, because they do not have the initial sequence corresponding to the N-terminal arm (residues 5−29).

ACKNOWLEDGMENT

The collaboration of the beamlines DW32 (LURE), X11 (DESY, Hamburg, Germany), and ID9 (ESRF) teams is gratefully acknowledged.

REFERENCES

1. Zannoni, D. (1989) *Biochim. Biophys. Acta 975*, 299−316.
2. Averill, B. A. (1996) *Chem. Rev. 96*, 2951−2964.
3. Zumft, W. G. (1997) *Microbiol. Mol. Biol. Rev. 61*, 533−616.
4. Ferguson, S. J. (1987) *Trends Biochem. Sci. 12*, 354−357.
5. Horio, T., Higashi, T., Sasagawa, M., Kusai, K., Nakai, M., and Okunuki, K. (1960) *Biochem. J. 77*, 194−201.
6. Yamanaka, T., Ota, A., and Okunuki, K. (1961) *Biochim. Biophys. Acta 53*, 294−308.
7. Kuronen, T., and Ellfolk, N. (1972) *Biochim. Biophys. Acta 275*, 308−318.
8. Silvestrini, M. C., Colosimo, A., Brunori, M., Walsh, T. A., Barber, D., and Greenwood, C. (1979) *Biochem. J. 183*, 701−709.
9. Wharton, D. C., Gudat, J. C., and Gibson, Q. H. (1973) *Biochim. Biophys. Acta 292*, 611−620.
10. Silvestrini, M. C., Tordi, M. G., Colosimo, A., Antonini, E., and Brunori, M. (1982) *Biochem. J. 203*, 445−451.
11. Vijgenboom, E., Busch, J. E., and Canters, G. W. (1997) *Microbiology (Reading, U.K.) 143*, 2853−2863.
12. Shimada, H., and Orii, Y. (1976) *J. Biochem. 80*, 135−140.
13. Greenwood, C., Barber, D., Parr, S. R., Antonini, E., Brunori, M., and Colosimo, A. (1978) *Biochem. J. 173*, 11−17.
14. Silvestrini, M. C., Tordi, M. G., Musci, G., and Brunori, M. (1990) *J. Biol. Chem. 265*, 11783−11787.
15. Fülöp, V., Moir, J. W. B., Ferguson, S. J., and Hajdu, J. (1995) *Cell 81*, 369−377.

16. Baker, S. C., Saunders, N. F. W., Willis, A. C., Ferguson, S. J., Hajdu, J., and Fülöp, V. (1997) *J. Mol. Biol. 269*, 440−455.
17. Williams, P. A., Fülop, V., Garman, E. F., Saunders, N. F. W., Ferguson, S. J., and Hajdu, J. (1997) *Nature 389*, 406−412.
18. Nurizzo, D., Silvestrini, M. C., Mathieu, M., Cutruzzolà, F., Bourgeois, D., Fülop, V., Hajdu, J., Brunori, M., Tegoni, M., and Cambillau, C. (1997) *Structure 5*, 1157−1171.
19. Bennet, J. M., Schlunegger, M. P., and Eisenberg, D. (1995) *Protein Sci. 4*, 2455−2468.
20. Bergdoll, M., Remy, M.-H., Cagnon, C., Masson, J.-M., and Dumas, P. (1997) *Structure 5*, 391−400.
21. Parr, S. R., Barber, D., Greenwood, C., Phillips, B. W., and Melling, J. (1976) *Biochem. J. 157*, 423−430.
22. Otwinovski, Z. (1993) *DENZO: an oscillation data processing program for macromolecular crystallography*, Yale University Press, New Haven, CT.
23. Bourgeois, D., Nurizzo, D., Kahn, R., and Cambillau, C. (1998) *J. Appl. Crystallogr. 31*, 22−35.
24. Brunger, A. T., Kuriyan, J., and Karplus, M. (1987) *Science 235*, 458−460.
25. Brunger, A. T. (1996) *X-PLOR Manual*, Yale University Press, New Haven, CT.
26. Read, R. J. (1986) *Acta Crystallogr. A42*, 140−149.
27. Roussel, A., and Cambillau, C. (1991) in *Silicon Graphics Geometry Partners Directory*, p 86, Silicon Graphics, Mountain View, CA.
28. Laskowski, R., MacArthur, M, Moss, D., and Thornton, J. (1993) *J. Appl. Crystallogr. 26*, 91−97.
29. Silvestrini, M. C., Falcinelli, S., Ciabatti, I., Cutruzzolà, F., and Brunori, M. (1994) *Biochimie 76*, 641−654.
30. Margoliash, E., and Frohwirt, N. (1959) *Biochem. J. 71*, 570−572.
31. Blatt, Y., and Pecht, I. (1979) *Biochemistry 18*, 2917−2922.
32. Cheesman, M. R., Ferguson, S. J., Moir, J. W. B., Richardson, D. J., Zumft, W. G., and Thomson, A. J. (1997) *Biochemistry 36*, 16267−16276.
33. Brucker, E. A., Olson, J. S., Ikeda-Saito, M., and Phillips, G. N., Jr. (1998) *Proteins 30*, 352−356.
34. Harutyunyan, E. G., Safonova, T. N., Kuranova, I. P., Popov, A. N., Teplyakov, A. V., Obmolova, G. V., Vainshtein, B. K., Dodson, G. G., and Wilson, J. C. (1996) *J. Mol. Biol. 264*, 152−161.
35. Ozawa, S., Sakamoto, E., Ichikawa, T., Watanabe, Y., and Morishima, I. (1995) *Inorg. Chem. 34*, 6362−6370.
36. Pettigrew, G. W., and Moore, G. R. (1987) in *Cytochromes c. Biological Aspects* (Rich, A., Ed.) Springer-Verlag, Berlin.

BI981348Y